Pulmonary lobar segmentation from computed tomography scans based on statistical shape model

Zhang, Y.[1], Osanlouy, M.[1], Clark, A.R.[1], Hoffman, E.A.[2], Tawhai, M.H[1]

[1]Auckland Bioengineering Institute, University of Auckland, Auckland, NZ, [2]Department of Radiology and Biomedical Engineering, University of Iowa Carver College of Medicine, Iowa City, IA, US.

Abstract

Automatic identification of pulmonary lobes from imaging is important in lung disease assessment and treatment planning. However, the pulmonary lobar fissure can be difficult to detect automatically, as it is thin, can often run close to the imaging plane, and can be obscured by or confused with features of disease. In this study, we aim to overcome difficulties in identifying pulmonary fissures by usinge a statistical shape model to guide lobar segmentation. By deforming an average lobar model onto an individual's lung shape, we predict fissure locations approximately, to refine our search region for lobar structures. Then, we use an eigenvalue of Hessian matrix analysis and a connected component eigenvector based analysis to determine a set of fissure-like candidate points. A smooth multi-level B-spline curve is fitted to the most fissure-like points (those with high fissure probability) and the fitted fissure plane is extrapolated to the lung boundaries. The method was tested on 20 inspiratory and expiratory CT scans in healthy young subjects and older subjects with idiopathic pulmonary fibrosis. A quantitative evaluation showed that the mean difference of left oblique, right horizontal and right oblique fissure to the reference was 2.06mm, 4.06mm and 2.85mm for healthy cases and 3.41mm, 5.79mm and 5.01mm for pathological cases.

1 Introduction

Human lungs are divided into five lobes which form distinct anatomical regions separated by a fissure~~, which are called the pulmonary lobes~~. ~~The extraction~~Identification of these lobes in imaging is of great importance for assessment of ~~in applications of~~ lung disease ~~assessment~~ severity and treatment planning [ref]. For clinical applications, the distribution and location of pulmonary disease are beneficial for doctors to recognize pathogenesis, guide therapy and have further value in surgical planning. The lobes are difficult to segment automatically as they can appear as faint or fuzzy lines in imaging, fissures can be incomplete (even in healthy patients), and there is anatomical variation in lobe shape and size between individuals [more refs(Gülsün et al 2006).]. This anatomical variation is ~~However, to find an effective and time-saving automatic lobe segmentation method is really challenging because of anatomical variation and incomplete fissures. On one hand, lobes vary between subjects. The anatomical variation of lobe is~~ usually associated with age, sex and body type [refs]. ~~Pathologies of diseased lungs usually deform the lobar shape abnormally and result in some fuzzy appearance of fissures on CT images. On the other hand, even in patients with healthy lung parenchyma the fissures are usually incomplete (Gülsün et al 2006).~~

In a broad sense,~~ the~~ existing algorithms that aim to automatically segment pulmonary lobes c~~omputational lobar segmentation methods usually c~~onsist of two steps: ~~the~~ lung segmentation and ~~the~~ fissure detection. Lung segmentation~~Currently, quite a number of~~ lung segmentation methods are well~~-~~established and results are typically reliable [refs]~~-~~. ~~to get a reliable result.~~ In

批注 [Office1]: Its more important here to explain why you are doing the study than to give all the technical details so you need some sentences along these lines.

带格式的：突出显示

批注 [Office2]: These two sentences effectively say the same thing and don't give a strong motivation for lobar segmentation. Papers I have found give lots of reasons which don't come across here (definitely needs more references and examples):

- Relative functional independence of lobes – because they are independent they logical way to divide the lung when assessing disease distribution, and are likely candidates for surgical removal
- Disease classification: Some diseases are almost exclusively localized to certain lobes of the lung, particularly in early stages, and being able to identify lobar distributions of abnormalities in imaging helps to diagnose pathology and understand the impact of certain pathologies on whole lung function (e.g. ventilation perfusion matching.
- Intra-patient registration: Lobes are important landmarks when registering within patient imaging (eg changes in lung tissue over time) and allow us to localize disease progression
- Operative planning: e.g. emphysema patients benefit most

...

批注 [Office3]: Body type? This is a vague term. Do you mean body fat percentage/BMI or height?

带格式的：突出显示

带格式的：突出显示

contrast, ~~most challenges for~~ automated ~~lobar segmentation lie in the~~ fissure detection is challenging [refs]~~even though a number of researches have been involved in~~. Some proposed fissure detection methods ~~One kind of fissure detection method~~ make~~s~~ use of either local or global knowledge of lung~~the~~ anatomy, ~~of lung structure~~ such as airway and vessel trees, to identify fissures [refs]. ~~based on two features of lungs. The first feature is the fact that there should~~For example, there ~~not be any~~ are not typically any large vessels in the vicinity of lobar fissures, so fissures should be located in the gaps between airway and vessel trees. These methods can be time consuming as airways and blood vessels must be identified as an intermediate step. ~~Another feature is the vessels and bronchi could be classified into five lobe regions using an edge detection method.~~ A second class of fissure detection algorithm ~~Another kind of method commonly~~ makes use of gray-level information and shape information to detect the fissures [ref]. Generally, lobar fissures can be regarded as bright planes crossing the pulmonary volume because of the higher density value of fissures comparing to the surrounding tissues [ref]. Based on this information, ~~quite a number of~~several published methods use local filtering algorithm to detect the voxels which lie on these planes, so that these detected voxel points can construct a continuous fissure surface ~~.~~(van Rikxoot et al 2008, Ukil and Reinhardt 2009, Lassen et al 2013, Ross et al 2010, Doel et al 2012). These algorithms often face problems when lobe fissures are blurry or incomplete.

In this paper, we propose a statistical shape model (SSM) guided method to segment pulmonary lobes from CT images. Our new procedure does not depend on prior segmentation of anatomical structures (airway lobar classification) and has promising potential as a clinically useful automatic lobe segmentation procedure. A user-interactive interface is also developed for user to control and visualize the whole segmentation process and, if necessary, do some manual correction on the segmentation results.

批注 [Office4]:

2 Methods

~~–~~We follow a three-step approach for lobe segmentation (Fig 1): in the first step, a threshold~~ing~~ based lung segmentation method ~~is developed to get the~~defines the lung boundary. In the second step, a statistical shape model is deformed ~~to get a~~provide a 'search region' for ~~of interest (ROI) of~~ fissure locations. In the third step, ~~the fissures are accurately~~fissures are located using ~~the~~ a Hessian matrix protocol combined with connected component filters and surface fitting algorithm. ~~This method is able to detect fissures in all subjects, whereas existing segmentation tools failed in several subjects. Our new procedure does not depend on prior segmentation of anatomical structures (airway lobar classification) and has promising potential as a clinically useful automatic lobe segmentation procedure. A user-interactive interface is also developed for user to control and visualize the whole segmentation process and do some manual correction on the segmentation results.~~

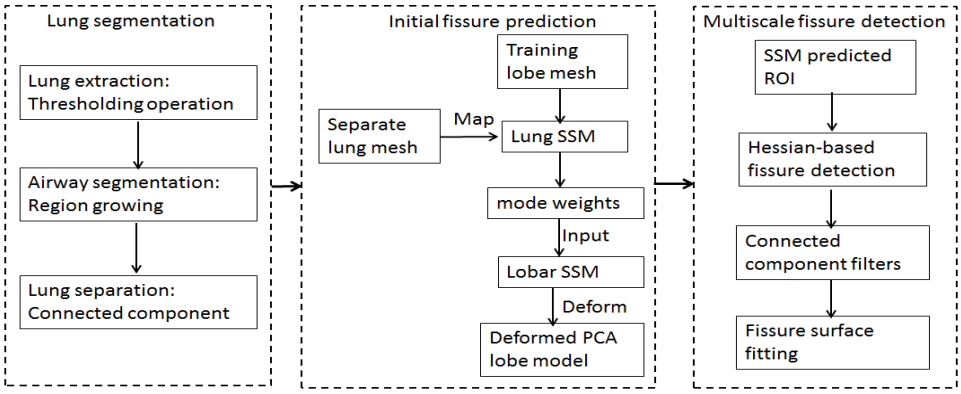

Fig. 1. Flow diagram of the lobar segmentation process.

3 ~~Method~~

2.1 Lung segmentation

~~A good lung segmentation is a prerequisite for the next steps in this study, since all the other segmentations need perform inside the two lung regions. In this paper, we used a common~~Here we use commonly used thresholding method to segment lungs [ref]. T~~, the procedure is consist of the following steps: T~~he method ~~firstly~~ uses a thresholding operation (-775 Hounsfield Units) and connected component identification to find ~~the initial~~an initial approximation to the lung regions and trachea location. Us~~inge~~ the ~~highest~~ most apical point of trachea as a start point, a region growing technique is applied to detect the airway trees. Then, left and right lungs are separated as the two largest connected components remaining after removing the trachea and main left and right bronchi. ~~Fig 2 shows the lung segmentation result.~~

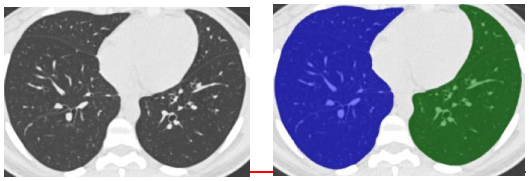

~~Fig. 2. Lung segmentation result. (a) Raw CT image. (b) Segmented lungs.~~

2.2 ~~Initial fissure prediction~~Active shape model of lung shape

~~In the last twenty years, statistical shape model (SSM) based method has been widely used as one of the most successful methods for medical image segmentation. SSM makes use of statistical analysis to model shape variation, thus can be used to model and capture the shape difference and the mean shape among different people..~~

~~In this paper,~~ A Statistical Finite element analysis of Lobe (SFeaL) which is based on ~~the~~ an a~~A~~ctive s~~S~~hape m~~M~~odel (ASM) of the lung is constructed and deformed onto the individual's images to predict ~~the~~ an initial fissure ~~locations for guiding the future accurate~~to guide fissure detection. The SFeaL model was constructed using a training set consisting of imaging of the lung … The open-source visualization software CMGUI (https://www.cmiss.org/cmgui) was employed to manually digitize all three fissure points between adjacent lobes by an expert user to provide a gold-standard fissure location for each subject in the training set.

~~This approach employs~~A finite element volume mesh is used to describe the shape of the lung

带格式的：行距：单倍行距
带格式的：两端对齐
批注 [Office5]: Here you need to describe the data that went into building the statistical shape model, including how fissures were segmented for these subjets
带格式的：突出显示
带格式的：突出显示

and its fissures both in terms of the ASM and also to define initial fissure location in the segmentation algorithm. A high order (bi-cubic Hermite) finite element mesh template was fitted to lung surface data obtained from the lung segmentation (Section 2.1). The template mesh for ~~to specify pulmonary lobar shape which provides an efficient parameterized representation of lobar boundaries and makes shape constraints available during image analysis. As any other statistical model guided segmentation, the first common step here is generating the statistical lobar mesh using a set of training data. To define lung shape, both left and right lung surface data cloud was created using the lung segmentation method introduced in section 2.1. The open source visualization software CMGUI (https://www.cmiss.org/cmgui) was employed to manually digitize all three fissure points between adjacent lobes. A high order (bi-cubic Hermite) finite element mesh template was then constructed for fitting the lung and fissure data cloud. By geometry fitting the surface data to the mesh, we are able to mathematically describe a three-dimensional subject-specific lung shape.~~ t~~T~~he left lung mesh has 35 nodes and 44 elements, while the right lung mesh has 50 nodes and 62 elements. Each node has 12 degrees of freedom (DoF) which store the global coordinates and first and second nodal derivatives. A least squares fit of the mesh to the lung surface data was conducted using ~~During the fitting process, a least square fitting optimization, which aimed to minimize the sum of the distances between each data point and its projection on to the nearest element was solved using~~ CMISS (https://www.cmiss.org), a ~~mathematical modeling~~finite element modeling environment. The average root mean square (RMS) error of this fitting method was 0.52mm ~~averagely on the~~for the 30 training subjects (Fig 3(a)).

批注 **[Office6]:** Do any nodes have defined anatomical locations, what is done to ensure they can be used as pseudo landmarks.

To construct the ASM, each node in the finite element mesh was used as a pseudo-landmark and a principal component analysis (PCA) conducted on the training set.

~~In the next stage, all the left and right nodes (85 nodes) were selected as pseudo landmarks to represent variations across the training cases.~~ To remove the orientation and scaling differences between shapes, a g~~G~~eneral p~~P~~rocrustes a~~A~~lignment (GPA) method was used to minimize the distance between ~~two~~ subjects through calculating the optimal rotation matrix and translation (Fig 3(b)) [ref]~~n~~. The volumes of all the subjects were normalized to 1L during the processing ~~(Fig 3(b))~~. The procrusted aligned meshes ~~can be represented using the following expression:~~is represented by

$$B = [\overline{x_1}\ \overline{y_1}\ \overline{z_1}\ \overline{x_2}\ \overline{y_2}\ \overline{z_2} \cdots \overline{x_p}\ \overline{y_p}\ \overline{z_p}],$$

w~~W~~here p is the total node number of all the subjects (2550 nodes for our study, 30 subjects in total), and the over-line represents GPA to the mean. The matrix B was then decomposed into modes of variation by a ~~Principal Component Analysis (~~PCA [ref]~~)~~. Each mode symbolizes one type of lobe shape variation. PCA is a statistical procedure using an orthogonal transformation to help us find the principle components, which here are the modes with the most lobar shape variation through analyzing the eigenvectors and eigenvalues of the covariance matrix of the data matrix B. The results of principle components of variation showed that the first seven principal components account for over 90% of the total variation. The PCA provides a definition of a statistically averaged lobar shape.

带格式的：突出显示

批注 **[Office7]:** If you are short of space some of this info could be removed.

带格式的：突出显示

2.2 Initial prediction of lobar location in an individual

~~Now average statistical lobar shape model has been constructed with principal component nodes defined.~~ To predict the fissure locations in ~~, a new~~ volumetric CT imaging from a subject ~~i~~not~~s chosen which should be separated from the~~part of the training cohort a finite element mesh of the lung surface (~~subjects. The lung surface FE mesh~~ without ~~the~~ fissure information) is generated ~~using the previous method~~for this subject. This l~~and this l~~ung surface mesh ~~was then~~is projected on to the PCA-trained average lung statistical mesh (no fissure surfaces). The principal component~~s'~~ weight values were calculated from the projection and these weights were then used on the deformation of PCA-trained average lobar statistical mesh (with fissure surfaces) to derive an initial estimation of fissure locations (Fig 3(c) (d)). This initial ASM based prediction of lobar fissures provides a reduced search area for subsequent image analysis and ensures definition of complete lobar structures even if a fissure is incomplete or difficult to detect in a small region of the image.

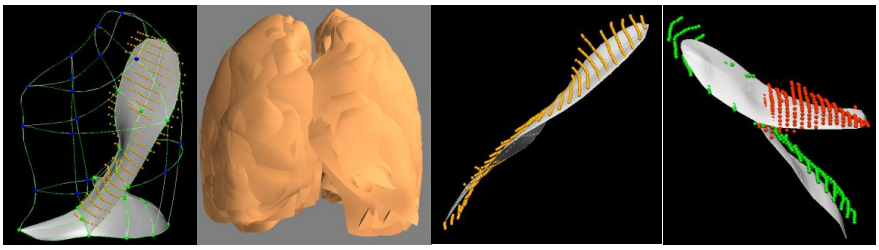

(a) (b) (c) (d)

Fig. 3. SSM based initial fissure prediction results. (a) Lung surface fitting and fissure digitizing manually. (b) Procrustes aligned meshes of 30 subjects. (c) (d) Fissure prediction compared to manual tracing points. White mesh is the predicted fissure surfaces.

2.3 Multiscale Hessian-based ~~multiscale~~ fissure detection

The location of ASM predicted fissure planes (Fig 3d) are used to guide a Hessian based fissure detection in an individual. ~~In 3D space, fissures can be regarded as plane-like structure, since the grey-value increases rapidly from the structure border to the center and decrease again to the opposite border. Multiscale Hessian-based filters are thus used to enhance and differentiate these structures with specific shapes, i.e., blobs, sheets and tubes, which significantly describe the second order derivative information of imaging. The original CT image here was first applied by a~~ Gaussian filters with a range of kernel sizes from 0.5mm to 2.5mm was applied to the image set. ~~Each~~ The responses at each ~~kernel size gets a response and all the responses are then~~are combined to get a maximum ~~one~~ response for each voxel of the image. This multiscale operation guarantees fissures of variable ~~a variety of sizes of fissures~~size can be captured by Hessian operations. At each image voxel, the Hessian matrix was constructed as a symmetric matrix. ~~Since for~~For a ~~-~~fissure structure, which presents as~~,~~ a light plane on a dark background ~~is characterized by~~ two large positive second derivatives across the plane and a small second derivative (of either sign) along the plane are expected. This is reflected in the Hessian matrix as two small eigenvalues corresponding to the eigenvectors along the fissure planes and one large eigenvalue perpendicular to the plane. Thus with ~~Thus fissures modeled as plane should be reflected by a Hessian matrix having two small eigenvalues corresponding to the eigenvectors along the fissure planes and a large eigenvalue, since there is a strong curvature perpendicular to the fissure. So on the bright fissures,~~ the relationship of eigenvalues λ_1, λ_2, λ_3 is defined as $|\lambda_1| \leq |\lambda_2| \leq |\lambda_3|$. λ_{31} is expected to ~~be~~ much larger than~~, while~~ λ_{12} and λ_{32} ~~are typically both low~~at the

批注 **[Office8]:** Can you specify how many and where they sit in the range if this is always the same

fissure. From these characteristics, we can get a fissure probability of each voxel derived as follows:

$S = \tau S_{plane} S_{wall}$.

~~The first factor suppresses points whose largest eigenvalue λ_3 is positive, since fissures are locally bright :~~

~~$\tau = \begin{cases} 1, \lambda_3 < 0 \\ 0, \lambda_3 \geq 0 \end{cases}$~~ ~~The first factor suppresses~~The parameter τ surpresses points whose largest eigenvalue λ_3 is positive, since fissures are locally bright , and is defined as:

$$\tau = \begin{cases} 1, \lambda_3 < 0 \\ 0, \lambda_3 \geq 0 \end{cases}$$

S_{plane} detects plane or curve-like structures by searching for locations where $|\lambda_3|$ and $|\lambda_2|$ are significantly different:

$$S_{plane} = \exp(-\frac{{S_{plane}}^2}{2p^2}), \quad R_{plane} = \frac{|\lambda_2|}{|\lambda_3|}$$

~~ince the largest eigenvalue $|\lambda_3|$ should be much larger than the other two eigenvectors, the second factor detects plane or curve-like structures by searching for locations where $|\lambda_3|$ and $|\lambda_2|$ are significantly different~~S_{wall} . The third factor suppresses signals of noise and~~such as~~ 'blob'-like structures~~, in contrast to plane-like fissures, have relatively large three eigenvalues. P and w are both set to 0.5 as thresholding in this study:~~

~~$S_{plane} = \exp(-\frac{{S_{plane}}^2}{2p^2}), \quad R_{plane} = \frac{|\lambda_3|}{|\lambda_3|}$~~

$$S_{wall} = \exp(-\frac{{R_{noise}}^2}{2w^2}), \quad R_{noise} = \sqrt{\lambda_1^2 + \lambda_2^2 + \lambda_3^2}$$

S then gives a high response to local ~~the sheet~~sheet-like ~~local structures like~~structures such as fissures and suppresses ~~all the other structures with low values~~other pulmonary structures. ~~The result of an~~An example of a fissure enhancement filter applied in an individual is shown ~~can be seen~~ in Fig 4(a).

Blood vessels, which appear as similar structures locally to fissures are ~~points should be~~ removed from the fissure enhanced result~~. The segmentation of vessels is achieved using a classical vessel segmentation metho d~~using prevousy described methods (Frangi et al 1998), which removes~~. It is also depend on a multiple scales (from 0.5mm to 3.0mm) Hessian-based enhanced filter, which similar to the fissure detection. The main difference is to detect the~~ tube-like structures with ~~like vessels, the relationship of Hessian eigenvalues λ_1, λ_2, λ_3 should be defined as~~ $|\lambda_1| \approx 0$, $|\lambda_1| \ll |\lambda_2|$, $|\lambda_2| \approx |\lambda_3|$~~.~~ (Fig 4(b))~~.~~

~~ shows the result after eliminating the vessel voxels.~~

The ~~initial~~ fissure location predicted by the ASM allows definition of a search region for the fissure (Fig. 4(c)). ~~average statistical shape model deformation gives us a region of interest (ROI) for an accurate fissure detection. The c~~Candidate points are selected within a certain distance of the initial fissure approximation~~, see Fig 4(c). It can help us remove most of the lung regions~~. ~~Since there are still some spurious responses such as small~~A ~~plane-like structures on the result, a~~ 2D, 4-neighborhood connected component filter and a 3D 6-neighborhood vector-based

带格式的：下标

批注 [Office9]: You have changed which one is the largest! Above I think it should be as I have changed it to be consistedn

批注 [Office10]: Technical ter,??

带格式的：突出显示

带格式的：两端对齐

批注 [Office11]: Define the distance

connected component filter are employed successively to eliminate ~~these~~ noise arising from small plane-like structures in this search region (Fig 4(d)). The vector-based connected component filter ~~takes the largest eigenvector of Hessian matrix into consideration, as~~uses the inner product of the normalised largest eigenvector of the Hessian matrix in adjacent voxels. These largest eigenvector ~~i~~s are perpendicular to the fissure plane, and their inner product provides ~~and it shows the orientation of fissure structure. The inner product of two adjacent normalized eigenvector is calculated as~~ a ~~criteri~~criterion for~~a of~~ component connection. ~~Considering the fact that~~ As fissure ~~the~~ curvature of a fissure is locally low, adjacent fissure voxels should have similar largest eigenvectors and thus large inner product values~~ion~~. ~~With applying the filters, all the small connected components whose volumes lower than a threshold are removed as noise from the 3D image, see Fig 4(d).~~

The detected points ~~detected~~ are then divided into a set of small subsections corresponding to different (x', y'). For each subsection, the point of the highest fissure probability (the highest S value) is selected as the finial candidate fissure point (Fig 4(e)). Then a continuous smooth fissure surface is generated using a B-spline method with a thin-plane spline and extrapolated to the lung boundaries, see Fig 4(f).

批注 **[Office12]:** X' and y' are undefined

批注 **[Office13]:** Cant see anything on 4e!

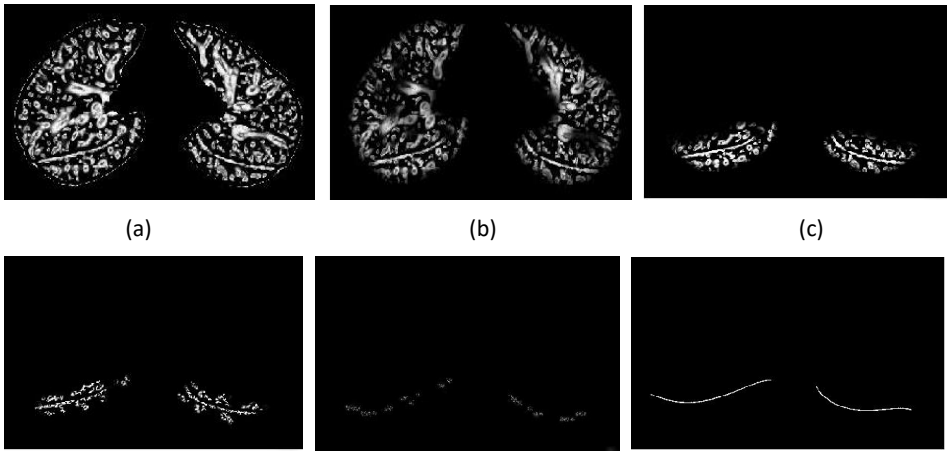

(a) (b) (c)

(d) (e) (f)

Fig.4. Hessian-based multiscale fissure detection results. (a) Hessian-based fissure enhancement. (b) Remove vessel voxels. (c) ROI of fissure locations based on SSM projection. (d) 2D and 3D eigenvector based connected component filter. (e) Fissure candidate points. (f) B-spline curve fissure surface fitting.

2.4 Interactive user control interface

For a successful lobar segmentation ~~As we discussed above,~~ a series of parameter values need to be defined. ~~chosen correctly to ensure a successful lobar segmentation.~~ However, one fixed value of parameter is usually not suitable for all the subjects due to a wide variation of lung tissue and fissure appearances across the population. Therefore, a fast and convenient interactive way to control the segmentation procedure ~~is reasonable and acceptable~~may be necessary on a case by case basis. Based on an open source Pulmonary Toolkit (PTK, https://github.com/tomdoel/pulmonarytoolkit), we developed an improved user-friendly interactive interface to control the segmentation parameters as input. By making use of some

批注 **[Office14]:** Please define specifically which parameter values

built-in objects and visualization system of PTK, we add our lobar segmentation algorithm into the algorithm package and make parameter control buttons available on the interface (Fig 5).

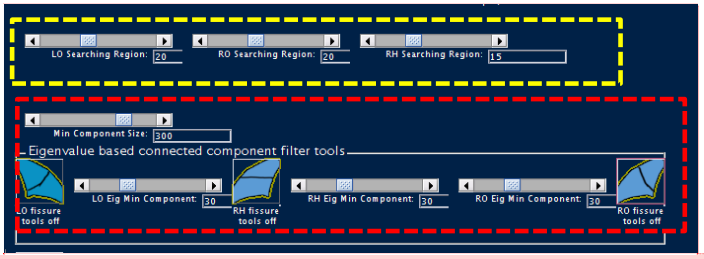

Fig. 5. User interactive interface. The yellow frame shows the slides for changing search region size of fissure detection, the red frame shows the slides for changing connected component sizes for each filter.

批注 **[Office15]:** Not easy to see.

批注 **[Office16]:** If we run out of space we should consider whether this is necessary. We are not providing anyone with the tools right now so it may be enough to say simply which parameters are image specific

批注 **[Office17]:** For Merryn to change but needs to be reworded

3 Experiment

3.1 Data

We tested our automatic lobar segmentation method on two ~~different kinds of~~ datasets : 1) CT images of young normal volunteers taken at different lung volumes and with different thickness 2) Clinical CT images of old patients diagnosed with idiopathic pulmonary fibrosis (IPF) disease.. ~~These normal~~Normal subjects are selected from Human Lung Atlas (HLA) dataset which is approved by the University of Iowa Institutional Review Board and Radiation Safety Committees. The selected subjects are consists of 5 functional residual capacity (FRC) cases and 5 total lung capacity (TLC) cases. Slice thickness was 0.5-0.7mm. ~~2) Clinical CT images of old patients diagnosed with idiopathic pulmonary fibrosis (IPF) disease.~~ These diseased subjects are acquired from Auckland District Health Board (ADHB) under the supervision of Dr. Wilsher, following ethics committee approval for this study. Slice thickness was 1.25-3mm.

3.1 Result

To assess the accuracy of the automatic lobar segmentation method in the normal and disease subjects, we compared the automatic segmentation results to gold-standard manual segmentations. ~~the manual ones with digitized all the three fissures.~~ Segmentation accuracy was quantitatively evaluated~~The fissure points were clicked on 2D cross sections and sagittal slices manually. The quantitative evaluation of the segmentation accuracy was assessed from~~ by computing the mean difference ~~difference and the~~and ~~percentile~~ percentage of fissure points <3mm~~measurement~~ between gold-standard and automatic segmentations. The ~~The mean difference is defined as the mean distance between each manual fissure point and its closet voxel in automatic lobar segmentations:~~

$$d_i^{min} = \min_j \left\{ \sqrt{(x_j^a - x_i^m)^2 + (y_j^a - y_i^m)^2} \right\}$$

$$d_{mean} = \frac{(\sum_{i=1}^{n} d_i^{min})}{n}$$

~~Where (x_i^m, x_i^m) is the manually-defined contour voxel location and (x_i^a, x_i^a) is a computer-defined contour voxel location. The quantitative analysis of the segmentation result is shown in Fig 6.~~

~~The percentile measurement is defined as the percentage of the distance between manual and automatic point under~~ 3mm criteria~~, following the equation:~~on

$$\sqrt{(x_i^a - x_i^m)^2 + (y_i^a - y_i^m)^2} \leq 3\text{mm}$$

since 3mm approximates the thickness of clinical CT images that surgeons and radiologists read in clinical settings [ref].

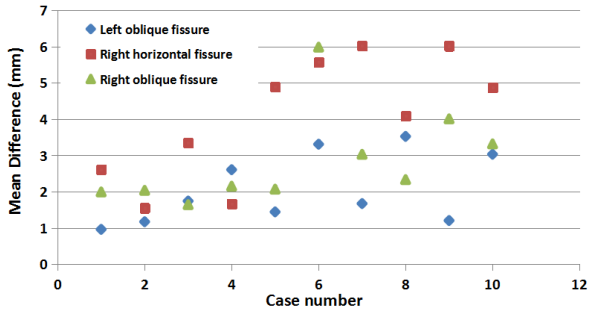

(a)

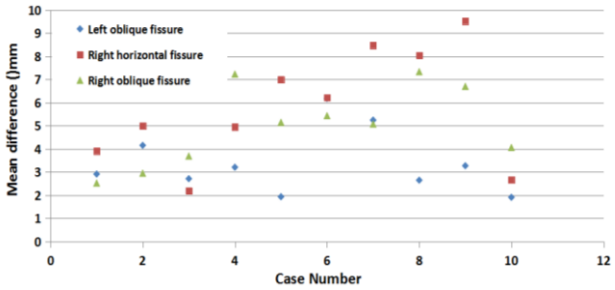

(b)

Fig.6. Quantitative evaluation results of the segmentation accuracy. (a) Mean difference of normal young subjects. (b) Mean difference of IPF old subjects.

The average mean difference assessed on normal subjects and IPF subjects are 2.06mm, 4.06mm, 2.85mm and 3.41mm, 5.79mm, 5.01mm for left oblique, right horizontal and right oblique fissure respectively. The average percentile accuracy on normal subjects and IPF subjects are 78.39%, 61.62%, 72% and 65.86%, 55.94%, 60.06% for left oblique, right horizontal and right oblique fissure respectively. List same info on IPF.

带格式的：突出显示

Due to the lower resolution and pathologic abnormalities, IPF subjects got a worse accuracy. In addition, the segmentation method performs well on left oblique fissure than right oblique fissure and right horizontal fissure, because left lung has simpler anatomic structure with only one fissure, in contrast, misdetection happens more often in the area of right lung where the two fissures are closed. See Fig 7, which shows the accuracy distribution of the three fissures with different colors. It can be seen that the method causes higher error in the lung boundary area, since the fissures here are commonly incomplete, thus few fissure candidate points can be detected accurately.

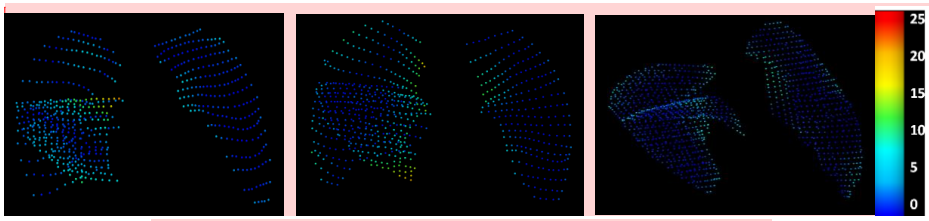

(a) (b) (c)

Fig.7. Accuracy distribution results of some example subjects.

Replace this using info on how parameters that can be controlled need to be altered for successful segmentation

~~In addition, current published studies show that it seems impossible to ensure one fully automatic lobar segmentation method perform perfectly on all kinds of subjects, especially for some diseased abnormal cases. Therefore, we developed a correction tool on the user interface to improve the result manually, as shown in Fig 8.~~

~~(a) (b) (c)~~

~~Fig. 8. Fissure manual correction procedure. (a) Fissures before correction, the blue region is the corrected region. (b) Fissures after correction. (c) The interface for operating correction.~~

4 Conclusions and Discussions

In this paper, we present an automatic pulmonary lobar segmentation method combined with some manual interaction. The result shows that our segmentation method can perform well on CT images of normal subjects and get a relative accurate result for most of the IPF abnormal subjects. In the future work, a statistical shape model dataset could be developed. The dataset could contain different kinds of statistical model for different ages, sexes, lung volume or diseases, since it can help us prediction a more accurate ROI for the future fissure detection. Meanwhile, the method need to be assessed on more diseased subjects and be improved combined with the disease characteristic of these images. A user-friendly interaction and more time-saving programming is also a key point in the future study.

Due to the lower resolution and pathologic abnormalities, IPF subjects got a worse accuracy. In addition, the segmentation method performs well on left oblique fissure than right oblique fissure and right horizontal fissure, because left lung has simpler anatomic structure with only one fissure, in contrast, misdetection happens more often in the area of right lung where the two fissures are closed. See Fig 7, which shows the accuracy distribution of the three fissures with different colors. It can be seen that the method causes higher error in the lung boundary area, since the fissures here are commonly incomplete, thus few fissure candidate points can be detected accurately.

批注 [Office18]: Cant see these images. If you dave directly as png from cmgui you should be able to get them on white backgrounds.

带格式的： 突出显示

带格式的： 两端对齐

批注 [Office19]: This section needs work.

1. What you have presented
2. Accuracy of mthod and comment on reduced accuracy in IPF, note that you can actually segment a fissure in IPF subject which many studies would not
3. Comparison to existing methods (why is it worth using yours)
4. Maybe at this point its appropriate to comment on gui in ptk but only if it is actually being added to the PTK repository for iothers to use
5. Touch briefly on study limitations.

Reference